Ferroelectric and optical properties of $Ba_{0.8}Sr_{0.2}TiO_3$ thin film

F. M. Pontes, E. R. Leite,[a] D. S. L. Pontes, and E. Longo
LIEC-CMDMC-Department of Chemistry-UFSCar, Via Washington, Km 235, CP-676, CEP-13565-905, São Carlos, S.P., Brazil

E. M. S. Santos, S. Mergulhão, P. S. Pizani, F. Lanciotti, Jr., and T. M. Boschi
Department of Physics, UFSCar-Via Washington, Km 235, CEP-13565-905, São Carlos, Brazil

J. A. Varela
Institute of Chemistry-UNESP-Araraquara, S. P., Brazil

(Received 4 October 2001; accepted for publication 11 February 2002)

Barium strontium titanate ($Ba_{0.8}Sr_{0.2}TiO_3$) thin films have been prepared on Pt/Ti/SiO_2/Si substrates using a soft solution processing. X-ray diffraction and also micro-Raman spectroscopy showed that the $Ba_{0.8}Sr_{0.2}TiO_3$ thin films exhibited a tetragonal structure at room temperature. The presence of Raman active modes was clearly shown at the 299 and 725 cm^{-1} peaks. The tetragonal-to-cubic phase transition in the $Ba_{0.8}Sr_{0.2}TiO_3$ thin films is broadened, and suppressed at about 35 °C, with a maximum dielectric constant of 948 (100 kHz). Electrical measurements for the prepared $Ba_{0.8}Sr_{0.2}TiO_3$ thin films showed a remnant polarization (P_r) of 6.5 $\mu C/cm^2$, a coercive field (E_c) of 41 kV/cm, and good insulating properties. The dispersion of the refractive index is interpreted in terms of a single electronic oscillator at 6.97 eV. The direct band gap energy (E_g) and the refractive index (n) are estimated to be 3.3 eV and $n = 2.27–2.10$, respectively. © *2002 American Institute of Physics.* [DOI: 10.1063/1.1466526]

I. INTRODUCTION

Ferroelectric thin films are potentially important materials for a variety of devices such as ferroelectric memories, infrared pyroelectric sensors and in other integrated technologies. Among the many classes of ferroelectric perovskites, the lead lanthanum titanate,[1] lead zirconate titanate,[2] lead titanate,[3] and barium titanate[4] have probably been the most intensively investigated. However, a serious problem of these materials is that they display polarization fatigue when subjected to electric field cycling. On the other hand, bismuth-layered perovskite, e.g., barium bismuth tantalate (SBT)[5] thin film, is reportedly a good candidate for nonvolatile ferroelectric random access memory since this film has good polarization and low fatigue characteristics. However, SBT films have a low dielectric constant and high crystallization temperature (~800 °C). A variety of processing techniques have been tried out to produce these thin films, including rf sputtering, sol gel, metalorganic chemical vapor deposition (MOCVD), laser ablation,[6–10] etc. On the other hand, barium strontium titanate (BST) is currently one of the most interesting ferroelectric materials due to its high dielectric constant and composition-dependent Curie temperature.

Many film growth techniques such as MOCVD,[11] sputtering,[12] molecular beam epitaxy,[13] laser ablation[14] have been employed to fabricate BST thin films. Actually, new solution deposition methods, based on wet chemistry, have been used for the preparation of oxide thin films. In this regard, chemical processing using solutions, including soft solution processing, have been attracting increased interest. The soft solution processing can be defined as an environmentally friendly processing using aqueous solution, and it seems to provide results similar to every other process using fluids such as vapor, gas, and plasma or beam/ vacuum processing, while consuming less total energy than other processing routes. In addition, it offers some advantages, such as homogeneity, stoichiometric control, and the ability to coat large area and complex substrates.

Among a few techniques of soft solution processing, the polymeric precursors method[15–17] can be included, because of the liquid nature of the constituents and the relatively low processing temperatures used, and this method yields products with much higher homogeneity than does solid-state processing.

Tahan, Safari, and Klein[18] reported BST thin films of various compositions by the sol-gel process, whose grain size ranged from 20 to 50 nm, and no ferroelectricity was present. However, there have been few reports on the ferroelectricity of the BST thin films. Yuzyuk *et al.*[19] reported polarized Raman spectra of tetragonally distorted ($Ba_{1-x}Sr_x$) TiO_3 ferroelectric films on a MgO substrate using a micro-Raman analysis.

From this viewpoint, this work reports $Ba_{0.80}Sr_{0.20}TiO_3$ thin films with good ferroelectricity, successfully fabricated by soft solution processing. The structure of the films was characterized using x-ray diffractometry (XRD), micro-Raman spectroscopy and scanning electron microscopy (SEM).

II. EXPERIMENT

The starting materials were barium carbonate ($BaCO_3$), strontium carbonate and titanium (IV) isopropoxide. Citric acid and ethylene glycol were used as the chelanting and

[a]Electronic mail: derl@power.ufscar.br

polymerizing agents, respectively. Titanium citrates were formed by the dissolution of titanium (IV) isopropoxide in a water solution of citric acid (60–70 °C) under constant stirring. Strontium carbonate was added, at a stoichiometric quantity, to the titanium citrate solution. After homogenization of the solution, resulting in a clear solution, $BaCO_3$ was slowly added, while stirring vigorously. In order to achieve total $BaCO_3$ dissolution, ammonium hydroxide was dropwise until the *p*H reached 7–8. After homogenization of the solution containing Sr and Ba cations, ethylene glycol was added to promote mixed citrate polymerization by the polyesterification reaction. With continued heating at 90 °C, the solution became more viscous. The relative proportion of the metallic ions present in the polymeric precursor solution was Ba/Sr/Ti equal to 0.8/0.2/1.0. The viscosity of the deposition solution was adjusted to 10 mPa/s by controlling the water content. Thin films were prepared by dipping platinum-coated silicon and quartz substrates in the previously described polymeric precursor solution and subsequently pulling it up at a constant speed of 0.76 cm/min. After deposition, each layer was dried at 150 °C on a hot plate for 20 min to remove residual solvents. The heat treatment was carried out in atmospheric air in two stages: initial heating at 400 °C for 2 h at a heating rate of 5 °C/min to burn the organic materials, followed soon thereafter by heating at 700 °C for 2 h for crystallization. Each layer was heat treated at 400 and at 700 °C before the next layer was coated. This process was repeated several times to produce the desired film thickness.

The thermal decomposition characteristics of the polymeric precursor solution were investigated by thermogravimetric analysis (TGA) and differential scanning calorimetry (DSC) (STA 409, Netzsch, Germany), in synthetic air (30 cm^3/min) using a constant heating rate of 10 °C/min from room temperature up to 800 °C. In this study, the gel was pre-dried at 100 °C for 6 h, and then analyzed.

The $Ba_{0.80}Sr_{0.20}TiO_3$ thin films were structurally characterized by x-ray diffraction (XRD) (Cu K_α radiation) in the mode of $2\theta-\theta$ scan, recorded on a Siemens D5000 diffractometer. The lattice parameters of the $Ba_{0.80}Sr_{0.20}TiO_3$ thin films were measured using the least- square method. The optical transmittance of BST films was measured in the wavelength range of 200–2500 nm using double beam UV-VIS-NIR spectrophotometer (Cary 5G – Varian). The micro-Raman measurements were performed at room temperature, using the 514.5 nm line of an argon ion laser as the excitation source. The power was kept at 15 mV and a 100 × lens was used. The spectra were recorded using a T-64 Jobin-Yvon triply-monochromator coupled to a conventional photon counting system.

The film thickness was measured by observing the cross section of the films by SEM using a Zeiss DSM940A scanning electron microscope (SEM). Atomic force microscopy (AFM) was used to obtain an accurate analysis of the sample surface and the quantification of very important parameters such as roughness and grain size. A Digital Instruments Multimode Nanoscope IIIa (Santa Barbara, CA) was used. AFM imaging was carried out in the contact mode, using a trianguar-shaped 200-μm-long cantilever with a spring constant of 0.06 N/m. The temperature dependence of the dielectric constant was measured in the films in a metal-ferroelectric-metal (MFM) configuration, using a HP4192A impedance/gain phase analyzer, and the hysteresis loop measurements were carried out on the films with a Radiant Technology RT6000HVS. These loops were traced using the ''Charge 5'' program included in the software of the RT6000HVS in a virtual ground mode test device. The characteristic leakage current-voltage (I–V) curve was measured using a voltage source measurement unit (Keithley 237). To measure electrical properties, Au dot electrodes of ~ 0.3 mm in diameter were deposited by sputtering through a designed mask onto the film surfaces. In order to achieve a contact with the platinum bottom electrode, a corner of the film was etched away using a HF + HCl mixing solution.

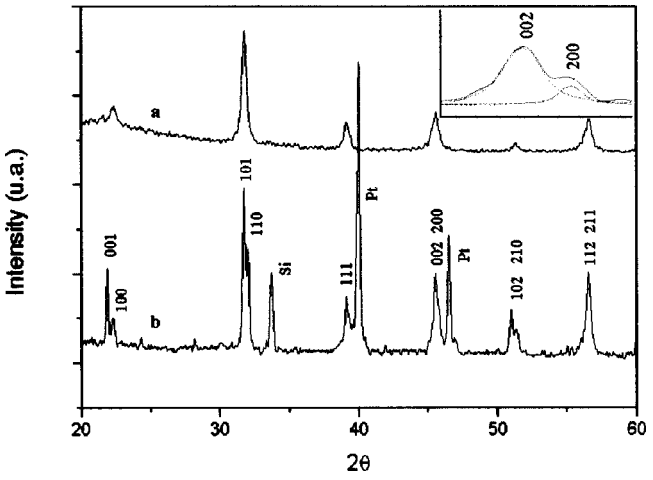

FIG. 1. XRD pattern of the soft solution processed $Ba_{0.8}Sr_{0.2}TiO_3$ thin film on (a) quartz and (b) platinum-coated silicon substrates. The inset shows the deconvolution of the {200/002} peaks on platinum-coated silicon substrate.

III. RESULTS AND DISCUSSIONS

XRD analysis revealed a tetragonal perovskite crystal structure with a distortion of ~1.018 for the $Ba_{0.8}Sr_{0.2}TiO_3$ thin film. Figure 1 displays XRD patterns of the films deposited on platinum-coated silicon and quartz substrates at 700 °C. The films were polycrystalline without preferential orientation and contained only the perovskite phase. The films derived from the polymeric precursor method showed obvious tetragonality, as evident from the distinct splitting of the {100/001} and {200/002} reflections (see inset of Fig. 1). In addition, no apparent splitting of (200) and (002) peaks was observed by Cheng *et al.*[20] for $Ba_{0.8}Sr_{0.2}TiO_3$ thin films by sol-gel process.

The thermolysis behavior of BST gel that had been predried at about 100 °C is shown in Fig. 2. TGA analysis indicated a major weight loss between 50 and 700 °C. No weight loss was observed at temperatures higher than about 700 °C, indicating that all organic material was burned, signifying final conversion to a ceramic powder. To verify the crystallization peak, pre-pyrolized powders of BST were calcined at 300 °C for 2 h. The TGA curve [Fig. 2(b)] shows a small weight loss of about 5%, between 50 and 200 °C, which corresponds to the evaporation of absorbed water, a major

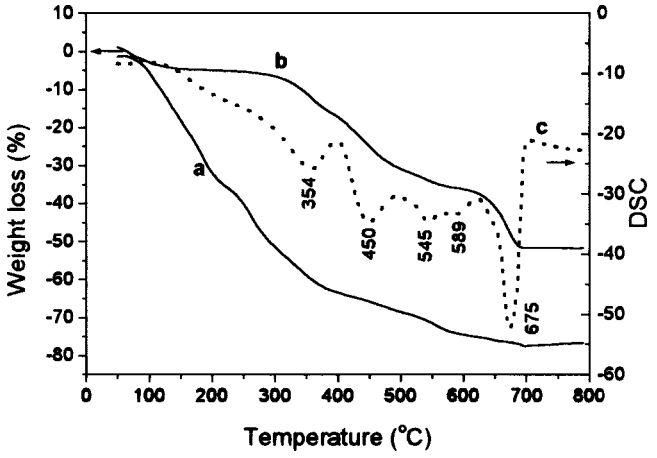

FIG. 2. DSC-TGA curves for: (a) TGA curve for gel sample; (b) TGA curve for pre-pyrolized powder; (c) DSC curve for pre-pyrolized powder.

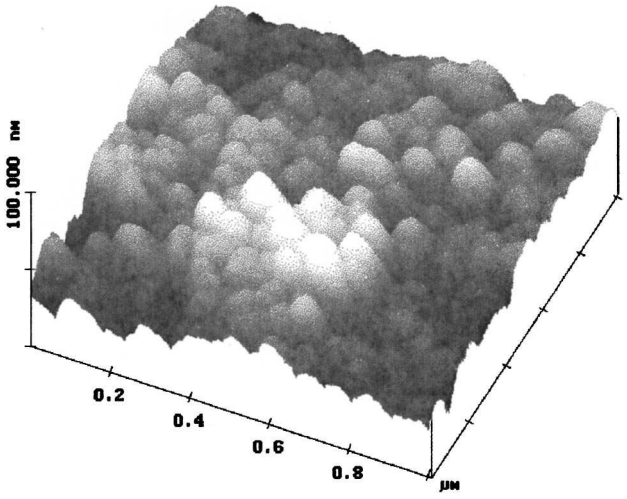

FIG. 4. AFM micrograph of BST film annealed at 700 °C.

weight loss (32%), between 300 and 600 °C, which is probably due to the drastic removal of carboxylic groups and their combustion, and a weight loss (12%) in the range of 600–690 °C. The final weight loss was completed at about 690 °C. Differential scanning calorimetry analysis carried out in the powder shows several exothermic peaks; no further changes beyond 690 °C were observed. The DSC data indicated exothermic peaks at about 354, 450, 545, and 584 °C, which were attributed probably to the loss/combustion of specific organics groups. The final DSC peak which appears at ~675 °C may be due to the final combustion of organics, associated with the crystallization temperature of the BST perovskite phase evidenced by the exothermal peak in the DSC curve and later confirmed by XRD.

The surface morphology of a polymeric solution derived $Ba_{0.8}Sr_{0.2}TiO_3$ thin film obtained by scanning electron microscopy is shown in Fig. 3. It can be seen from this figure that large grains with a size of about 100 nm were formed in BST film. The film thickness is approximately 400 nm verified by SEM. The average grain size and the surface roughness of the BST thin film were also estimated using atomic force microscopy. Figure 4 shows the images of BST thin film annealed at 700 °C for 2 h, which was characterized by a small surface roughness with a uniform, crack-free microstructure, which is in agreement with the SEM analysis. The average grain size and surface roughness (rms) of the spherical shaped grains were calculated using the equipment's software routine. The average grain size and the surface roughness were close to 90 and 4.5 nm, respectively.

The micro-Raman spectra measured at room temperature after having the film annealed at 700 °C are shown in Fig. 5 together with the labeling of the positions of Raman shifts, according to the convention explained in Refs. 21 and 22. All peaks were attributed to the Raman active modes from the perovskite structure of the $Ba_{0.8}Sr_{0.2}TiO_3$ film. The peaks at wave number around 230, 297, 517, and 724 cm^{-1} are identified as $A_1(2TO)$, $E(3TO+2LO)+B_1$, $A_1(3TO)$, and $E(4LO)$,[23] respectively. The micro-Raman spectrum from the film with four frequency peaks is similar to that of the tetragonal $BaTiO_3$ crystal.[24] These peaks in the films shifted slightly toward lower wave numbers as compared with those in the powder and $BaTiO_3$ single crystal, indicating the ex-

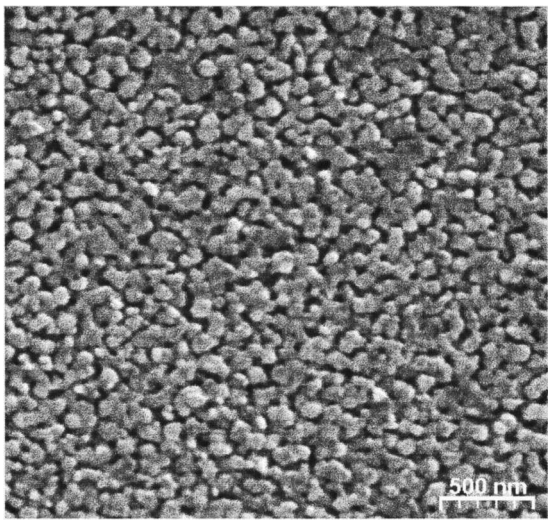

FIG. 3. SEM micrograph of the $Ba_{0.8}Sr_{0.2}TiO_3$ thin film prepared by soft solution process.

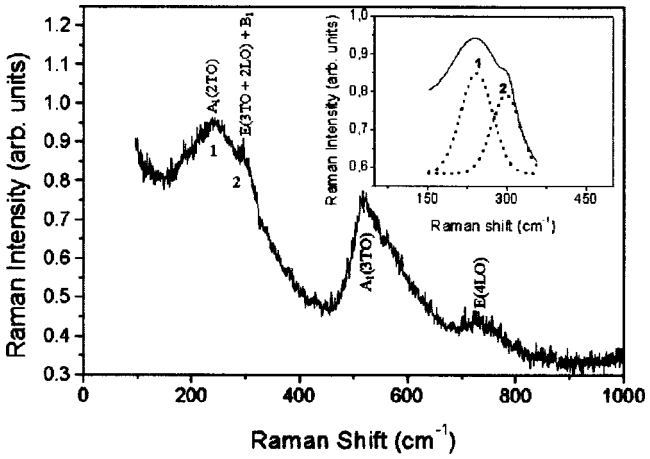

FIG. 5. Micro-Raman spectrum of the $Ba_{0.8}Sr_{0.2}TiO_3$ thin film prepared by soft solution process.

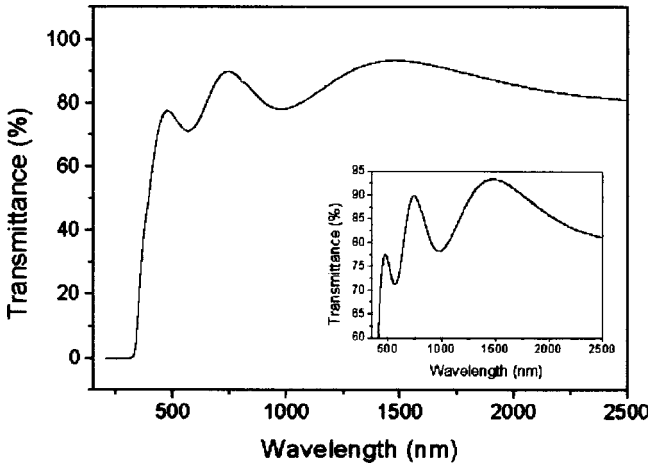

FIG. 6. The optical transmission spectrum of a $Ba_{0.8}Sr_{0.2}TiO_3$ thin film annealed at 700 °C.

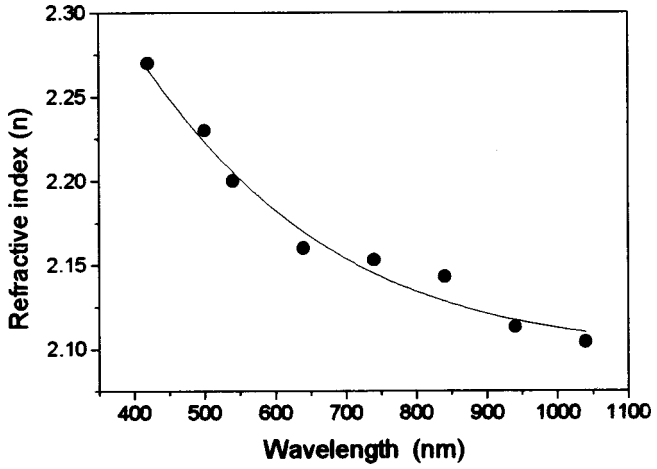

FIG. 7. The relationship between refractive index of $Ba_{0.8}Sr_{0.2}TiO_3$ thin film and wavelength.

istence of tensile stress in the film. A similar phenomenon has commonly been observed by other authors.[25]

Examining the important features of the $Ba_{0.8}Sr_{0.2}TiO_3$ film spectrum in order of increasing wave number, a broadband at $\sim 241\ cm^{-1}$ is observed. Next is a narrow peak at $\sim 299\ cm^{-1}$. An intense broadband at $\sim 517\ cm^{-1}$ is skewed toward the high frequency side, in a manner similar to the corresponding band in the $BaTiO_3$ single crystal.[24] The highest frequency peak, at $\sim 725\ cm^{-1}$, corresponds to the $728\ cm^{-1}$ peak seen in the $BaTiO_3$ single crystal spectrum.[24]

As discussed above, the micro-Raman spectra provide unambiguous confirmation of the presence of the tetragonal ferroelectric phase of $Ba_{0.8}Sr_{0.2}TiO_3$ thin film through the observation of the Raman peaks at ~ 299 and $\sim 725\ cm^{-1}$. Similar results have been reported in BST film prepared by the sol-gel method.[26] The Raman spectrum upon excitation of active modes reveled that soft solution processed $Ba_{0.8}Sr_{0.2}TiO_3$ thin film has good crystalline and tetragonal structure.

Figure 6 shows the optical transmission spectrum of a $Ba_{0.8}Sr_{0.2}TiO_3$ thin film annealed at 700 °C. The film has a perovskite structure confirmed by XRD and micro-Raman spectroscopy. The film was highly transparent and colorless to light at wavelengths longer than 460 nm. The high transmittance indicates low surface roughness and relatively good homogeneity of the film. In addition, the transmission drops rapidly at 420 nm, and the cutoff wavelength occurs at 320 nm. The interference fringes are a result of the interference between the air-film and film-substrate interfaces.

Optical constants like refractive index (n) of the film, have been determined from the transmittance spectrum following the method proposed by Manifacer, Gasiot, and Fillard.[27]

Refrective index values at different wavelengths were calculated from the wavelength spacing of adjacent extrema of the interference oscillations observed in the transmittance spectrum of $Ba_{0.8}Sr_{0.2}TiO_3$ film. Figure 7. shows the dispersion of the refractive index. The dispersion rises sharply with decreasing wavelength, showing the typical shape of a dispersion curve near an electronic interband transition.[28] The strong increase in the refractive index is associated with the fundamental band gap absorption. The curve shows that the refractive index follows the Cauchy function

$$n(\lambda) = a + \frac{b}{\lambda^2}, \tag{1}$$

where a and b are constants.

The dispersion data of the refractive index have been interpreted with a single electronic oscillator model.[29] Similar results have been observed in BST films prepared by other techniques.[30,31] Therefore, the dispersion of the refractive index can be described by the Sellmeier dispersion formula

$$n(\lambda)^2 - 1 = \frac{S_0 \lambda_0^2}{\left[1 - \left(\frac{\lambda_0}{\lambda}\right)^2\right]}, \tag{2}$$

where S_0 is the oscillator strength and λ_0 the average oscillator position.

As shown in Fig. 8, a plot of $1/(n^2-1)$ vs $1/\lambda^2$ gives a straight line, and fits the Sellmeier dispersion formula with a single electronic oscillator well. S_0 and λ_0 are deduced from the slope $(-1/S_0)$ of the resulting straight line and from the infinite wavelength intercept $[(1/S_0\lambda_0^2)]$, respectively. The average interband-oscillator energy (E_0) can be given by

$$E_0 = \frac{hc}{\lambda_0}, \tag{3}$$

where h is Planck's constant and c is the velocity of light.

Values of E_0, S_0, E_0/S_0 and λ_0 obtained in this work for $Ba_{0.8}Sr_{0.2}TiO_3$ film are reported in Table I and are compared with those reported for other authors.

The optical band gap of film can be determined from the sharply falling transmission region. The low-wavelength absorption data for $Ba_{0.8}Sr_{0.2}TiO_3$ film prepared on quartz substrates is related to the fundamental absorption assuming a direct transition between valence and conduction band (i.e., band-to-band transition). According to Tauc's law,[32] the absorption coefficient has the following energy dependence:

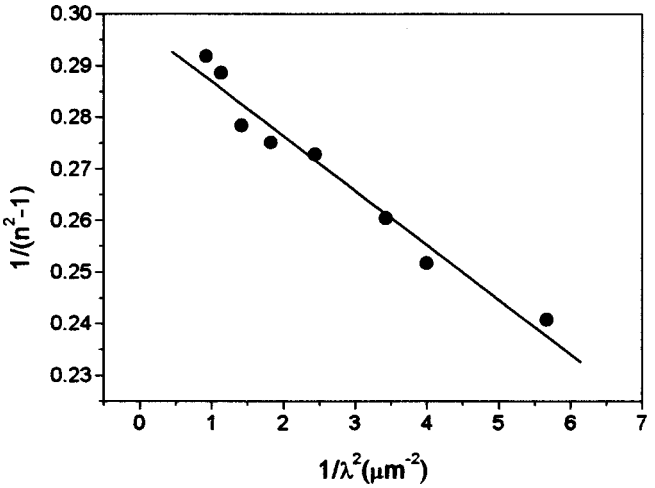

FIG. 8. Plot of $1/(n^2-1)$ vs $1/\lambda^2$ for $Ba_{0.8}Sr_{0.2}TiO_3$ thin film.

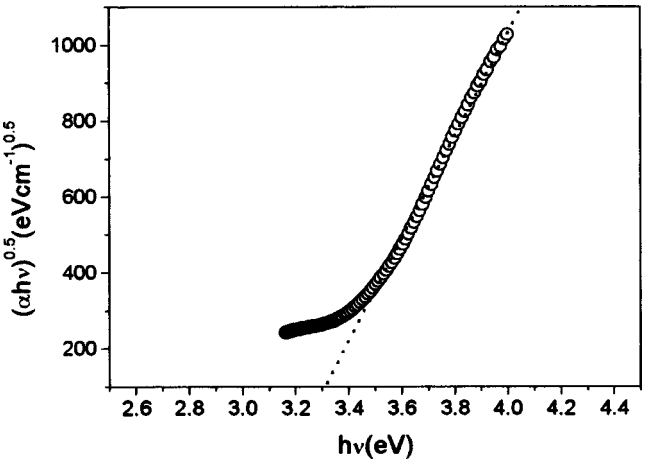

FIG. 9. The $(\alpha h\nu)^{1/2}$ vs $h\nu$ plot for $Ba_{0.8}Sr_{0.2}TiO_3$ thin film.

$$\alpha = B(h\upsilon - E_g)^2/h\upsilon. \tag{4}$$

The $(\alpha h\upsilon)^{1/2}$ vs $h\nu$ plots for the film are shown in Fig. 9. By extrapolating the linear portion of these curves to zero absorption $[(\alpha h\upsilon)^{1/2}=0]$, the calculated energy gap was about 3.3 eV which is close to the energy gap (3.31 eV) of $Ba_{0.8}Sr_{0.2}TiO_3$ film reported by Panda *et al.*[30] The energy gap from this work is reported in Table I and it is compared with the energy gaps elsewhere reported for BST films of diverse compositions.

The ferroelectric property of the $Ba_{0.8}Sr_{0.2}TiO_3$ thin film was examined in MFM configuration. Figure 10 gives the ambient temperature $P-E$ characteristics of the BST film. A well saturated *P-E* hysteresis loop is obtained with a remnant polarization of 6.5 $\mu C/cm^2$ and a coercive field of 41 kV/cm. The temperature dependence of the dielectric constant ($\epsilon_r - T$) curve in the $Ba_{0.8}Sr_{0.2}TiO_3$ thin film is displayed in Fig. 11. The dielectric constant was calculated from the capacitance, which was measured at 100 kHz and zero bias, using the following equations:

$$\epsilon_r = Ct/\epsilon_0 A, \tag{5}$$

where ϵ_0 is the permittivity of vacuum space, t is the film thickness, and A is the area of a top electrode. The temperature range for the $\epsilon_r - T$ test was from -258 to 125 °C. As the temperature changed, a dielectric constant peak appeared in the $\epsilon_r - T$ curve. The peak at about 35 °C was relatively sharp as shown in the inset of Fig. 11, which corresponds to a tetragonal-to-cubic phase transition. In addition, Cheng *et al.*[33] reported that the tetragonal-to-cubic phase transition temperature of the $Ba_{0.8}Sr_{0.2}TiO_3$ thin film prepared by sol-gel method was located at about 40 °C. O'Neill *et al.*[34] reported that ferroelectrics BST thin films with a grain size ~30–50 nm have a Curie temperature attributed to an tetragonal-to-cubic phase transition at ~15 °C. The dramatic variation in Curie temperature can be related to the small grain size. A comparison with the bulk $Ba_{0.8}Sr_{0.2}TiO_3$ ceramics shows that the peak was broadened and shifted to lower temperatures. It was reported that bulk $Ba_{0.8}Sr_{0.2}TiO_3$ ceramics showed a peak located at ~80 °C, which corresponds to a tetragonal-to-cubic phase transition.[34] It is well known that the properties of polycrystalline ferroelectrics are dependent on microstructure, particularly with respect to grain size. Zheng *et al.*[35] pointed out that the tetragonal-to-cubic phase transition temperature of the bulk BST ceramics is strongly dependent on the grain size if the crystallite size is lower than 500 nm. Lines and Glass[36] studied the bulk BST ceramic dependence of T_c or ϵ and suggested that T_c was greatly dependent on crystallite size.

TABLE I. Characteristic parameters of the optical functions of the BST polycrystalline thin films.

Material	$S_0(m^{-2})$	E_0(eV)	E_0/S_0(eV m^2)	$\lambda_0(\mu m)$	E_g(eV)
$Ba_{0.5}Sr_{0.5}TiO_3$[c]	1.04×10^{14}	7.16	6.9×10^{-14}	···	3.96
$Ba_{0.7}Sr_{0.3}TiO_3$[b]	···	5.87	···	···	3.50
$Ba_{0.8}Sr_{0.2}TiO_3$[d]	···	···	···	···	2.80
$Ba_{0.8}Sr_{0.2}TiO_3$[a]	10^{14}	6.76	6.76×10^{-14}	···	3.31
$Ba_{0.8}Sr_{0.2}TiO_3$ (This work)	0.945×10^{14}	6.97	7.37×10^{-14}	0.178	3.30

[a]Reference 30.
[b]Reference 31.
[c]Reference 37.
[d]Reference 38.

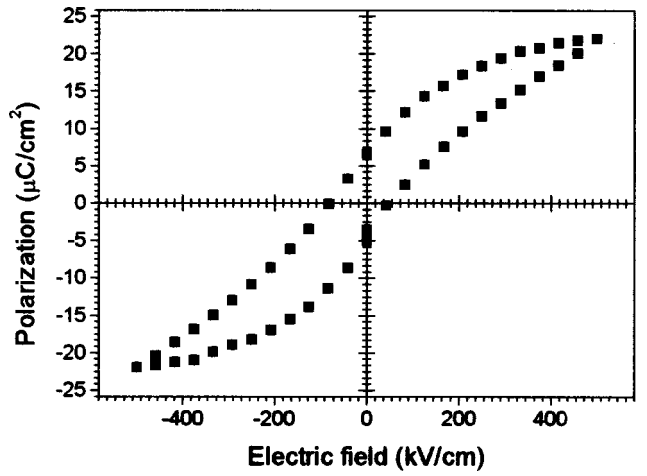

FIG. 10. *P - E* hysteresis loop of the soft solution processed $Ba_{0.8}Sr_{0.2}TiO_3$ thin film.

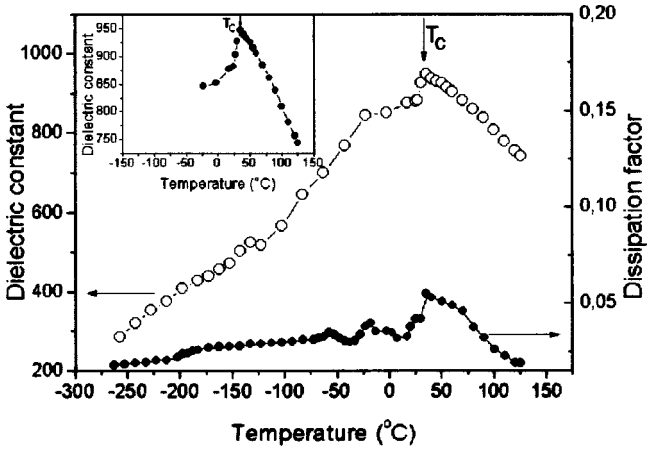

FIG. 11. The temperature dependence of dielectric constant and dissipation factor for $Ba_{0.8}Sr_{0.2}TiO_3$ thin film. The inset shows the variation of the dielectric constant in more details.

Figure 12 illustrates the current-voltage characteristics obtained for the BST film. At an applied voltage of 3 V, the leakage current density was approximately 3.3×10^{-7} A/cm^2. The low current density of the BST film capacitors demonstrates that the soft solution chemical process derived $Ba_{0.8}Sr_{0.2}TiO_3$ thin film has good insulating properties.

IV. CONCLUSION

We have studied the microstructure, optical and electrical properties of $Ba_{0.8}Sr_{0.2}TiO_3$ thin films, deposited onto the platinum- coated silicon and quartz substrates, derived from a soft chemical solution process. Micro-Raman spectroscopy was used to examine the structure of BST thin film. Micro-Raman spectra of the films were compared with spectra of single-crystal $BaTiO_3$ specimens and narrow peaks at 299 and 725 cm^{-1} were seen in the spectra, which are specific to tetragonal structure. Also, x-ray diffractometry investigation showed that the film contained only the perovskite phase and exhibited a tetragonal structure at room temperature. Scanning electron microscopy revealed grain size of 100 nm.

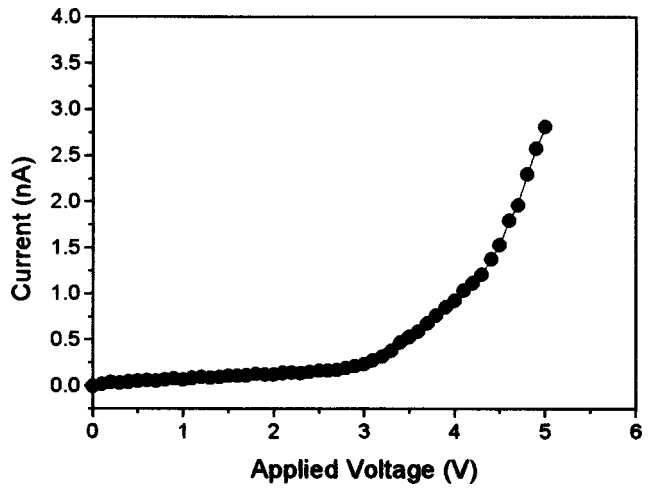

FIG. 12. Current vs applied voltage for the soft solution processed $Ba_{0.8}Sr_{0.2}TiO_3$ thin film.

From the transmission spectrum recorder in the range 200–2500 nm, the refractive index $n(\lambda)$ was determined. The dispersion of the refractive index was interpreted successfully in terms of a single electronic oscillator whose energy and strength are 6.97 eV and 0.945×10^{-14} m^2, respectively. The band gap energy of the $Ba_{0.8}Sr_{0.2}TiO_3$ polycrystalline film onto quartz substrate was found to be 3.3 eV from linear fitting of the absorption coefficient α to the Tauc plot of $(\alpha h\nu)^{1/2}$ vs ν. The temperature dependence of dielectric constant measurement showed that the $Ba_{0.8}Sr_{0.2}TiO_3$ thin film exhibited a tetragonal-to-cubic phase transition at about 35 °C. Electrical measurements for the film showed a remnant polarization of 6.5 μC/cm^2, a coercive field of 41 kV/cm, a low dissipation factor, and good insulating properties.

ACKNOWLEDGMENTS

The authors gratefully acknowledge the financial support of the Brazilian financing agencies FAPESP, CNPq/PRONEX and CAPES.

[1] S. Bhaskar, S. B. Majumder, P. S. Dobal, R. S. Katiyar, and S. B. Krupanidhi, J. Appl. Phys. **89**, 5637 (2001).
[2] J. Cheng and Z. Meng, Thin Solid Films **385**, 5 (2001).
[3] C. H. Wang and D. J. Choi, J. Am. Ceram. Soc. **84**, 207 (2001).
[4] H. Kumazawa and K. Masuda, Thin Solid Films **353**, 144 (1999).
[5] C. H. Lu and C. Y. Wen, Mater. Lett. **38**, 278 (1999).
[6] S. Kim and S. Baik, J. Vac. Sci. Technol. A **13**, 95 (1995).
[7] C. R. Cho, Mater. Sci. Eng., B **64**, 113 (1999).
[8] D. L. Kaier, M. D. Vaudin, L. D. Rotter, Z. L. Wang, J. P. Cline, C. S. Hwang, R. B. Marinenko, and J. G. Gillen, Appl. Phys. Lett. **66**, 2801 (1995).
[9] S.-B. Xiong, S. Migita, H. Ota, and S. Sakai, Mater. Lett. **38**, 406 (1999).
[10] M. Brazier, M. McElfresh, and S. Mansour, Appl. Phys. Lett. **72**, 1121 (1998).
[11] K. Abe and S. Komatsu, J. Appl. Phys. **77**, 6461 (1995).
[12] F. Techeliebou and S. Baik, J. Appl. Phys. **80**, 7046 (1996).
[13] Y. C. Choi, J. Lee, and B. S. Lee, Jpn. J. Appl. Phys., Part 1 **36**, 6824 (1997).
[14] D. M. Tahan, A. Safari, and L. C. Klein, J. Am. Ceram. Soc. **79**, 1593 (1996).
[15] M. P. Pechini, US Patent No. 3,330,697 (1967).
[16] F. M. Pontes, J. H. G. Rangel, E. R. Leite, E. Longo, J. A. Varela, E. B. Araújo, and J. A. Eiras, Thin Solid Films **366**, 232 (2000).
[17] P. S. Pizani, E. R. Leite, F. M. Pontes, E. C. Paris, J. H. Rangel, E. J. H. Lee, E. Longo, P. Delega, and J. A. Varela, Appl. Phys. Lett. **77**, 824 (2000).
[18] D. M. Tahan, A. Safari, and L. C. Klein, J. Am. Ceram. Soc. **79**, 1593 (1996).
[19] Y. I. Yuzyuk, A. Almeida, M. R. Chaves, V. A. Alyoshin, I. N. Zakharchenko, and E. V. Sviridov, Phys. Status Solidi **222**, 535 (2000).
[20] J. G. Cheng, X. J. Meng, J. Tang, S. L. Guo, and J. H. Chu, Appl. Phys. A: Mater. Sci. Process. **70**, 411 (2000).
[21] G. Burns and B. A. Scott, Phys. Rev. Lett. **25**, 1191 (1970).
[22] G. Burns, J. A. Sanjurjo, and E. Lopez-Cruz, Phys. Rev. B **30**, 7170 (1984).
[23] J. D. Freire and R. S. Katiyar, Phys. Rev. B **37**, 2074 (1988).
[24] L. H. Robins, D. L. Kaiser, L. D. Rotter, P. K. Schenck, G. T. Stauf, and D. Rytz, J. Appl. Phys. **76**, 7487 (1994).
[25] Y. I. Yuzyuk, R. Farhi, V. L. Lorman, L. M. Rabkin, L. A. Sapozhnikov, E. V. Sviridov, and I. N. Zakharchenko, J. Appl. Phys. **84**, 452 (1998).
[26] J. G. Cheng, J. Tang, X. J. Meng, S. L. Guo, and J. H. Chu, J. Am. Ceram. Soc. **84**, 421 (2001).
[27] J. C. Manifacer, J. Gasiot, and J. P. Fillard, J. Phys. E **9**, 1002 (1976).
[28] M. Wohlecke, B. Marrello, and A. Onton, J. Appl. Phys. **48**, 1748 (1977).
[29] S. H. Wemple and M. Didomenico, Phys. Rev. B **3**, 1338 (1971).
[30] B. Panda, A. Dhar, G. D. Nigam, D. Bhattacharya, and S. K. Ray, Thin Solid Films **332**, 46 (1998).
[31] Y. P. Wang and T. Y. Tseng, J. Mater. Sci. **34**, 4573 (1999).

[32] J. C. Tauc, *Amorphous and Liquid Semiconductor* (Plenum, New York, 1974), p. 159.
[33] J. G. Cheng, X. J. Meng, B. Li, J. Tang, S. L. Guo, J. H. Chu, M. Wang, H. Wang, and Z. Wang, Appl. Phys. Lett. **75**, 2132 (1999).
[34] D. O'Neill, G. Catalan, F. Porras, R. M. Bowman, and J. M. Gregg, J. Mater. Sci.: Mater. Electron. **9**, 1991 (1998).
[35] L. Zheng, W. L. Zhong, C. L. Wang, P. L. Zhang, and Y. G. Wang, J. Phys. D **32**, 546 (1999).
[36] M. E. Lines and A. M. Glass, *Principles and Applications in Ferroelectrics and Related Materials* (Clarendon, Oxford, UK, 1977), p. 531.
[37] F. Tcheliebou, H. S. Ryu, C. K. Hong, W. S. Park, and S. Baik, Thin Solid Films **299**, 14 (1997).
[38] H. F. Cheng, J. Appl. Phys. **79**, 7965 (1996).